Published in: ***Materials Science and Engineering A, 528 (2011) 2581-2591***

Microstructure Development and Hardening during High Pressure Torsion of Commercially Pure Aluminium: Strain Reversal Experiments and a Dislocation Based Model

Jiuwen Zhang[1,2], Nong Gao[1], Marco J. Starink[1]

[1]Materials Research Group, School of Engineering Sciences, University of Southampton, Southampton SO17 1BJ, United Kingdom
[2]School of Materials Science and Engineering, Dalian University of Technology, Dalian, China, 116085

Abstract

The effect of strain reversal on hardening due to high pressure torsion (HPT) was investigated using commercially pure aluminium. Hardening is lower for cyclic HPT (c-HPT) as compared to monotonic HPT (m-HPT). When using a cycle consisting of a rotation of 90° per half cycle, there is only a small increase in hardness if the total amount of turns is increased from 1 to 16. Single reversal HPT (sr-HPT) processing involves torsion in one direction followed by a (smaller) torsion in the opposite direction. It is shown that a small reversal of 0.25 turn (90°) reduces hardness drastically, and that decrease is most marked for the centre region. These behaviours and other effects are interpreted in terms of the average density of geometrically necessary dislocations (GNDs) and statistically stored dislocations (SSDs). A model is presented that describes the experimental results well. A key element of the model is the assumption that at the very high strains developed in severe plastic deformation processes such as HPT, the dislocation density reaches a saturation value. The model indicates that the strength / hardness is predominantly due to GNDs and SSDs.

Keywords: Severe Plastic Deformation (SPD); aluminium alloys; high pressure torsion; dislocation; hardness

1. Introduction

Severe plastic deformation (SPD) techniques have attracted much attention recently due to their ability to refine the grains in polycrystalline materials down to the micrometre and even to

nanometre level [1]. Grain refinement is dependent of not only alloy compositions but also the strain paths applied during SPD processing and different SPD methods impart different strain paths. Popular SPD methods include equal channel angular extrusion (ECAP) [2 , 3], accumulative roll bonding (ARB) [4], cyclic extrusion and compression (CEC) [5], multidirectional forging (MF) [6], and high pressure torsion (HPT) [7,8]. Recently developed SPD methods include high pressure tube twisting (HPTT) [9,10] and twist channel angular pressing (TCAP) [11].

HPT is a deformation procedure in which materials constrained between two anvils are subjected to SPD by torsional straining. One of the important features in HPT is that the sample can be deformed by introducing a rapid accumulation of high strain without interruption of straining other than by discontinuous processes like in other SPD processes [3,4,5,6]. Another one is that after initial compression by applied pressure there is no significant change in the size (thickness) and shape of disk during subsequent torsion strains [12]. There are a few reports on reversal deformation using HPT [13,14,15,16,17] (the words 'reversal deformation' is used to distinguish 'strain path' from strain paths in other SPD processes), but the mechanisms at the scale of dislocation movement are not fully understood.

HPT is different from most SPD processes (e.g. ECAP and ARB) in that substantial strain gradients are generated which should result in both an inhomogeneous microstructure as well as the formation of geometrically necessary dislocations (GNDs) (see e.g. [18,19,20]), whilst also extensive vacancies are generated [21]. Thus the study of HPT processing affords the possibility of studying these GNDs in conjunction with very high strains (>5) that are produced in a controlled manner. To date, very limited work referring to GNDs during HPT are available (see [22,23,24]), and there are no models that predict hardening due to HPT that incorporate GNDs. Several computationally intensive methods use the evolution of cell walls [23,25], and strain gradient effects (through the inclusion of GNDs) have been incorporated to model HPT [23]. Also a model of grain fragmentation based on lattice curvature has recently appeared [26]. But these models have as yet not been used to provide mechanical property predictions, and have not been tested against measured strength or hardness.

The objective of the present investigation is to analyse microstructural development and hardening during HPT, and provide a model that captures the main mechanisms for the

hardening due to GNDs, statistically stored dislocations (SSDs) and grain refinement. To this end we will perform an extensive range of HPT experiments including a range of strain reversal experiments. We will present a model of the microstructure and hardness evolution of Al–1050 during HPT. As will be demonstrated, the results of this investigation provide important new information on the development of hardness during HPT processing by presenting that there is a link between microstructure evolution and the changes of the density of GNDs and SSDs in HPT. The model also has relevance for other SPD processes.

2. Materials and experimental procedures

Commercially pure Aluminium (Al–1050) was selected for this investigation. Two batches of Al–1050 (A and B) were used and their compositions are shown in Table 1. (Both batches are well within specification of Al-1050. The second batch, batch B, had to be obtained as we ran out of material before we could complete all experiments.) Prior to HPT the Al–1050 had been extruded into a rod of 10 mm in diameter with grain size of 45 μm. The average Vickers microhardness (Hv) in this (as-received) condition is 30±2 Hv for Al-1050A and 33±2 Hv for Al-1050B, respectively. (This small difference is barely significant, and is swamped by the hardening introduced by HPT processing.) The specimens for HPT having a diameter of 10 mm were machined from extruded rod and mechanically ground to a thickness of 0.8 mm.

HPT processing was conducted at room temperature. No lubricant was applied on the sample, but some was applied on the anvil section adjacent to the sample. In the present experiments the pressure imposed on the sample between the two anvils is set at 3 GPa. The upper anvil is fixed and the lower anvil rotates to impose torsional straining on the HPT sample. Throughout a rotation speed of 1 rpm was used. The specimens were deformed using three types of HPT processing methods.

Alloy	Composition, wt%					
	Mg	Cu	Mn	Fe	Si	Al
Al–1050A	0.01	0.009	0.007	0.18	0.12	Bal.
Al–1050B	–	0.008	0.005	0.26	0.14	Bal.

Table 1 Compositions of the alloys studied

In order to provide clear descriptions of the three types of HPT processing methods, we will term the conventional HPT (also called monotonic HPT or m-HPT in abbreviation) as x_1T (Fig. 1a), where x_1 is the total turns of HPT and T represents a full revolution of 2π (i.e. 1 turn or 360º). The cyclic HPT (c-HPT) is designated as x_1T(c_x_2T) (Fig. 1b), where x_2 is the turns of per half cycle (here taken to be between 0.25 and 2, i.e. between 90º and 720º). For example, 16T(c_0.5T) denotes that the specimen is strained to a rotation of π (i.e. ½ turn or 180º) in forward direction and then in backward direction to π, and this cycle is repeated again and again until the required turns of 16 is attained. (Thus 16T(c_0.5T) consists of 16 cycles incorporating 31 direction reversals.) The direction change is near immediate (within a second). In the present investigation, 1T(c_0.25T), 16T(c_0.25T), 16T(c_0.5T), 16T(c_1T) and 16T(c_2T) were employed. The third type of tests is single reversal HPT (sr-HPT) processing (shown in Fig. 1c), in which one forward rotation is followed by a smaller counter rotation. In all the present sr-HPT tests, the forward direction was 16 turns. The number of backward direction turns is designated x_3. The tests are designated as 16T_x_3T.

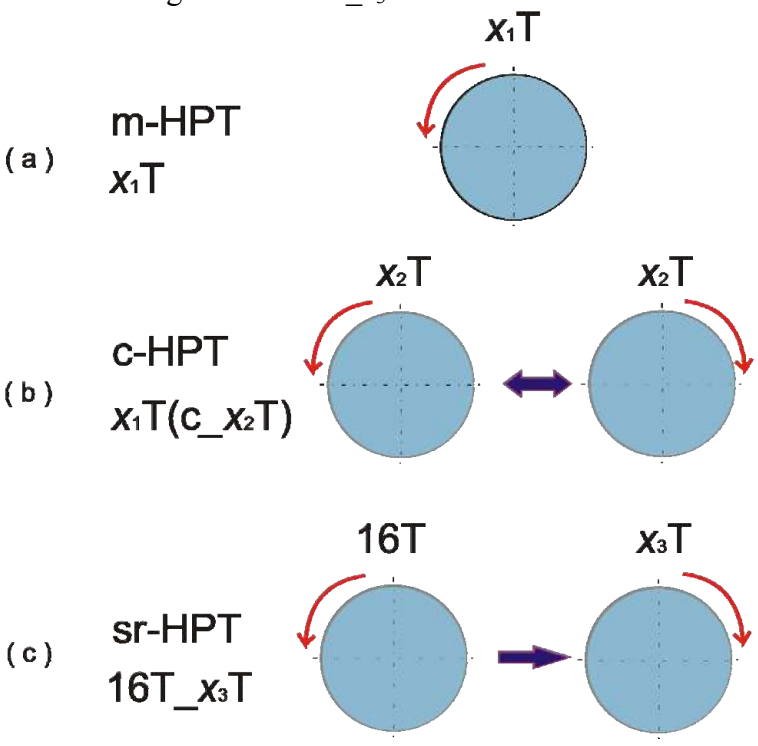

Fig. 1 Schematic illustrations of different HPT processes: (a) monotonic (m-HPT), (b) cyclic (c-HPT) and (c) single reversal (sr-HPT) processes.

Following HPT, selected disks of Al-1050A were cut into halves and cold mounted in order to characterize cross sections. The sections were carefully ground up to 4000-grit SiC paper and polished to a mirror-like finish by using a 0.05μm colloidal silica suspension. The Vickers microhardness, Hv, was measured at about 30 positions across a line through the centre of cross section of the disks by imposing a load of 200g for 15s. (For the centre region 50g load was used). For each reported Hv value typically three indentations were made. (Except at the centre on the cross section, where the minimum Hv was used.)

For Al-1050B, samples were cold mounted. After grinding and polishing by the same procedures like in Al-1050A, hardness tests were conducted on the entire broad (circular/disk) faces, where the Hv was recorded across at least four evenly aligned lines through the centre of broad surface (i.e. at least 121 Hv points were made). Error bars on graphs of these data represent the standard deviations. To make the presentation clearer, only selected error bars, representing typical standard deviations, are given.

To plot data as a function of equivalent strain and the total equivalent strain is calculated according to [27]:

$$\varepsilon = (2/\sqrt{3})\ln[(1+\gamma^2/4)^{1/2} + \gamma/2] \quad (1)$$

where γ is shear strain. For HPT experiments, the shear strain is given by

$$\gamma = 2\pi Nr/h \quad (2)$$

where N is the number of rotations, r is the distance of site of microhardness measurement from the centre of the sample and h is its thickness.

TEM was conducted on HPT processed alloy Al–1050B. (It is assumed throughout that the small differences in composition between the two batches do not significantly influence the TEM data, beyond some small change in the amount of Fe and Si containing particles.) The HPT processed discs were first ground to ~ 200 μm in thickness and then TEM samples of 3 mm in diameter were punched out at about 1 mm and 4 mm positions from the centre of the disks. Subsequently, the samples were thinned to perforation using two-jet electropolishing at -

30 ºC with an electrolyte solution of HNO_3: Methanol =1:3 (in volume). TEM foils were examined using a JEOL 3010 microscope operating at 300 kV.

3. Results

3.1 The microhardness of disks processed by m-HPT

Hardness data from m-HPT processed samples of Al–1050A are shown in Fig. 2a. Most HPT processed samples show an area of lower hardness near the centre of the sample. We will define this 'lower hardness zone' as the zone in which the hardness is 5% or more below the averaged hardness over the hardest 50% of the disc. It can be seen that the size of the lower hardness zone at the centre of disks shrinks as the total number of HPT turns is increased, and significant rises of hardness at centre regions of the disks can be observed (Fig. 2a). Just outside the lower hardness zone the hardness seems to be slightly higher than other parts of the disk when the total turns by HPT are more than 1, i.e. there is a local maximum in the hardness. This could be due to the interaction of increasing dislocation density with increasing radius, and recovery, which becomes dominant after dislocation densities reach a certain critical value. In the periphery of disks the hardness is more homogeneous and shows a slight increase with increasing total turns up to the maximum of 10 turns.

3.2 The microhardness of disks processed by c-HPT

Fig. 2b shows the diametric distribution of microhardness of the Al–1050B alloy processed by c-HPT and m-HPT for a total of 1 turn and 16 turns. (To make the presentation clearer, only selected error bars are given.) For the c-HPT experiments, the hardness across the disks generally increase with increasing strain per cycle, i.e. the hardness increases in the sequence 16T(c_0.25T), 16T(c_0.5T), 16T(c_1T), 16T(c_2T), and increases further to the 16T m-HPT processed sample. After a total turn of one full revolution, the hardness appears to have reached a saturation level in the periphery of disks (Fig. 2b), which is in agreement with the results in Fig. 2a. (It is noted that the Al–1050B alloy has a somewhat higher hardness as compared to the Al–1050A alloy. This is consistent with earlier observation that a slight change in Fe and Si content has a significant influence on hardness of disks after HPT [24].)

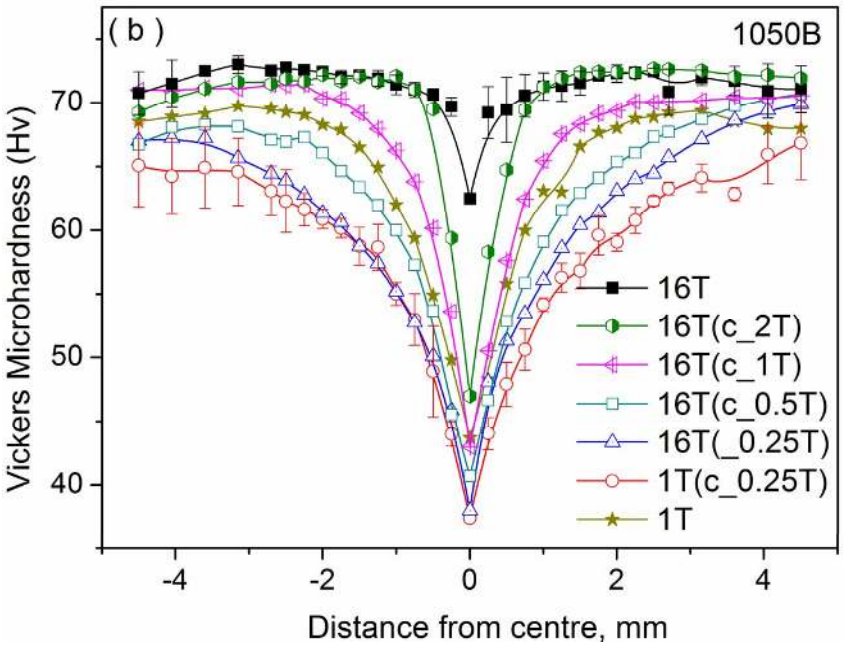

Fig. 2 Vickers microhardness vs. distance from the centre of disk for (a) Al–1050A processed by m-HPT for different total turns, and (b) Al–1050B processed by c-HPT for a total turn of 1 and 16 and a comparison with m-HPT.

In Fig. 2b, the Hv for c-HPT processed samples are also compared with those from the samples processed by m-HPT for 1 turn and 16 turns. For the c-HPT processed samples, little change in hardness was observed across the diameter when total deformation of the disks was increased from 1T(c_0.25T) to 16T(c-0.25T), i.e. the additional sixty 90º turns in alternating directions hardly increases the hardness beyond that achieved after four 90º turns in alternating directions. In the centre no increase in hardness can be detected at all. This is very different from m-HPT processed samples, where hardness in the centre increased dramatically from 43 Hv to 63 Hv when comparing 1T and 16T. This shows that c-HPT is very inefficient in increasing hardness as compared to m-HPT. Remarkably, in the centre the hardness of the disk processed by 16T(c_0. 5T) (i.e. 32 segments of 0.5 a turn in alternating directions) was even lower than by 1T. These data show the much reduced workhardening rate during the c-HPT process as compared to the m-HPT process.

In one c-HPT experiment the effect of dwell time on the strain reversal was checked. This involved samples processed by 1T(c_0.25T) with immediate strain direction change and with an

interval of 60s under compression between changing strain direction. No significant difference in hardness of the processed disks was observed.

3.3 The microhardness of disks processed by sr-HPT

It is considered that, if the GNDs dominate the strengthening at and near the centre of the HPT processed disk, reversal strains immediately imposed on the sample can be expected to reduce the hardness more at and near the centre than other regions (see Discussion). To investigate this we subjected disks to single reversal HPT (sr-HPT), by straining for 16 turns in forward direction and subsequently straining in the opposite direction for up to 5 turns. Fig. 3a shows the microhardness of the disks subjected to this processing. Comparison of data for the 16T (m-HPT) and the 16T_0.25T (i.e. straining as in 16 turns m-HPT followed by 0.25 turns in the reverse direction) samples, shows that the rotation of 0.25 turns in the opposite direction caused a drastic reduction in hardness over the entire sample, and the reduction of hardness is especially large in the lower hardness zone around the centre of the specimen. On increasing the amount of reversal deformation to 16T_0.5T, 16T_1T, 16T_2T, 16T_3T, and 16T_5T, the hardness gradually increased again. The increase slows down considerably, and there is nearly no further strengthening in disks processed from 16T_3T to 16T_5T. Also, this reduction/increment of hardness doesn't seem to vary with increasing radius except at and near the centre. The hardness did not recover to the hardness level of the 16T m-HPT processed sample, even though a strain of up to 5 turns was employed continuously in the opposite direction.

The change in Hv as a function of reversal strain (x_3T) in sr-HPT processing, plotted as a function of r, is shown in Fig. 3b. (x_3 = 0.25, 0.5, 1, 2, 3 and 5). With increasing the number of reversal turns from 0.25 to 5 by sr-HPT, all the curves show a similar trend that can be divided two stages: the drop stage of the hardness where the hardness suddenly drops and the rise stage of the hardness where the hardness rises. It should be noted that near the centre the rise stage of the curve is continuous (with near constant slope) over the investigated range of reversal turns, indicating the increase of strengthening due to GNDs is about proportional to the number of reversal turns. However, for areas away from the centre, the curves become flatter; suggesting the significant influence of SSDs on hardness in the outer regions of HPT processed disks (see

Discussion). Fig. 4 presents a comparison of the hardness variations of disks by three different HPT procedures and indicates the significant influence of m/c/sr-HPT on strengthening.

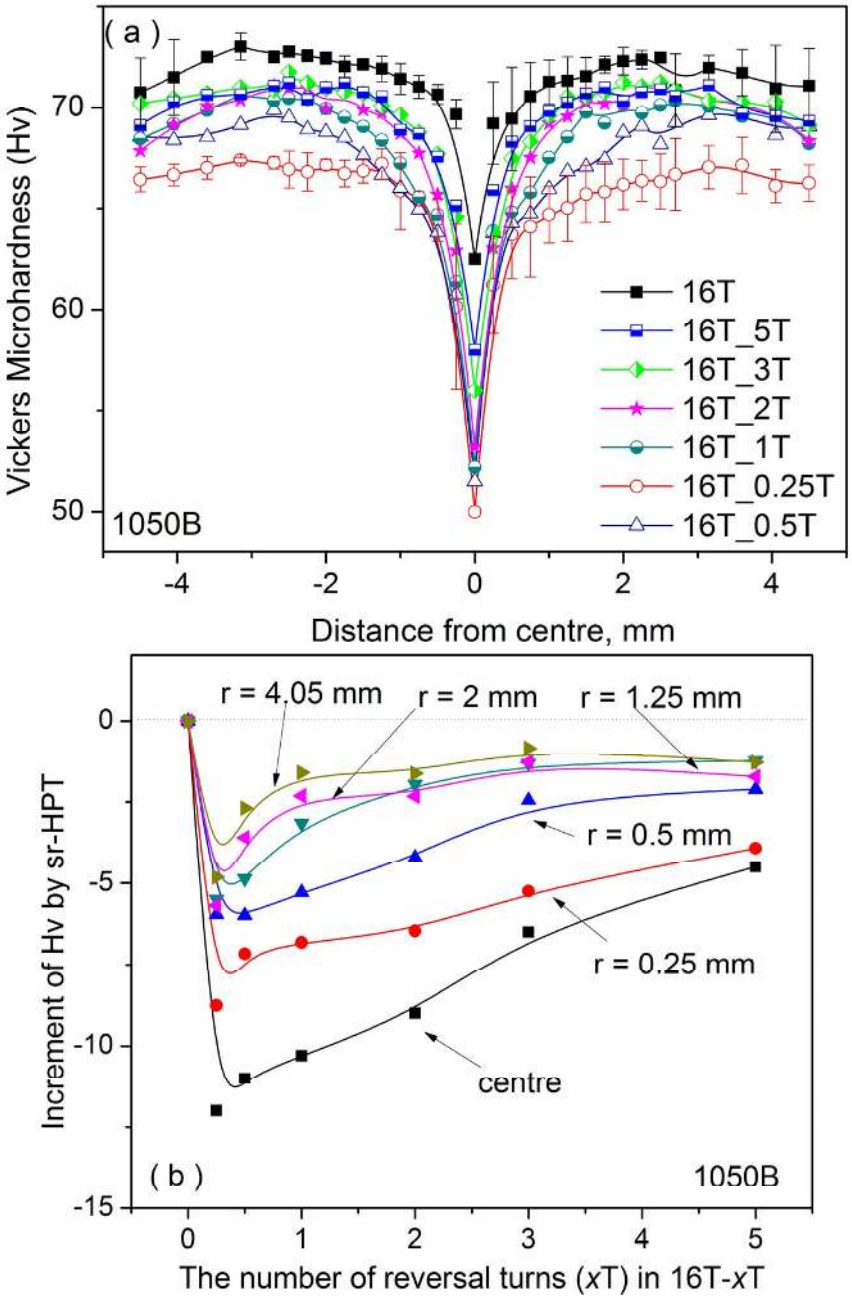

Fig. 3 (a)Vickers microhardness vs. distance from the centre of disks for Al–1050B after 16 turns by m-HPT and 16_x_3T by sr-HPT; (b) the increment of microhardness at different radius of the disk vs. the number of reversal turns (x_3T) for Al–1050B disks processed by sr-HPT for 16T_ x_3T.

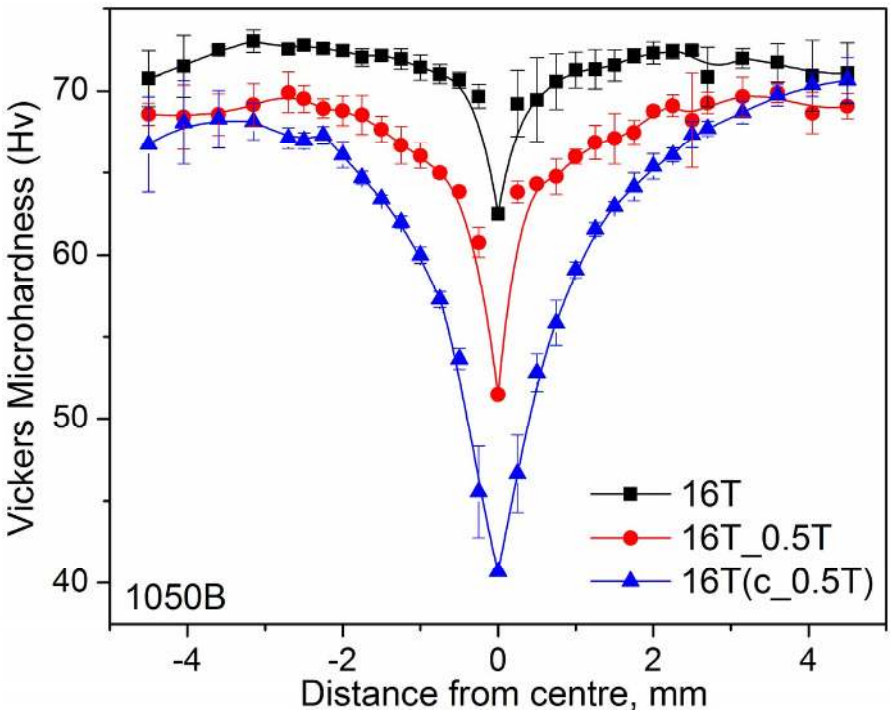

Fig. 4 A comparison of Vickers microhardness vs. distance from the centre of disks for Al–1050B processed by different HPT processes for a total of 16 turns.

3.4 Microstructural observations of disks subjected to HPT

TEM micrographs of Al–1050B alloy are shown in Fig. 5. Fig. 5a and b present the microstructure at about 1 mm ($\varepsilon_{eq} \approx 2.4$) and 4 mm ($\varepsilon_{eq} \approx 4$) from the centre of the disk subjected to 1T(c_0.25T) process, respectively. Fig. 5c and d show the result at about 1 mm ($\varepsilon_{eq} \approx 5.6$) and 4 mm ($\varepsilon_{eq} \approx 7.1$) from the centre of the disk subjected to 16T(c_0.25T) process. Coarser grains were observed near the centre of disks (Fig. 5a and c). Averaging over several TEM micrographs provided a grain size of 2.2 μm at about 1 mm from the centre of the disk processed for 1 turn and 2 μm for 16 turns, respectively. There is very little difference in grain sizes in the outer regions of both disks and the grain sizes measured is about 0.9 μm. After c-HPT for 16 turns the centre of the disk shows a slightly higher density of dislocations and more smooth and straight grain boundaries than for 1 turn (compare Fig. 5c to Fig. 5a), where the grain boundaries are thicker.

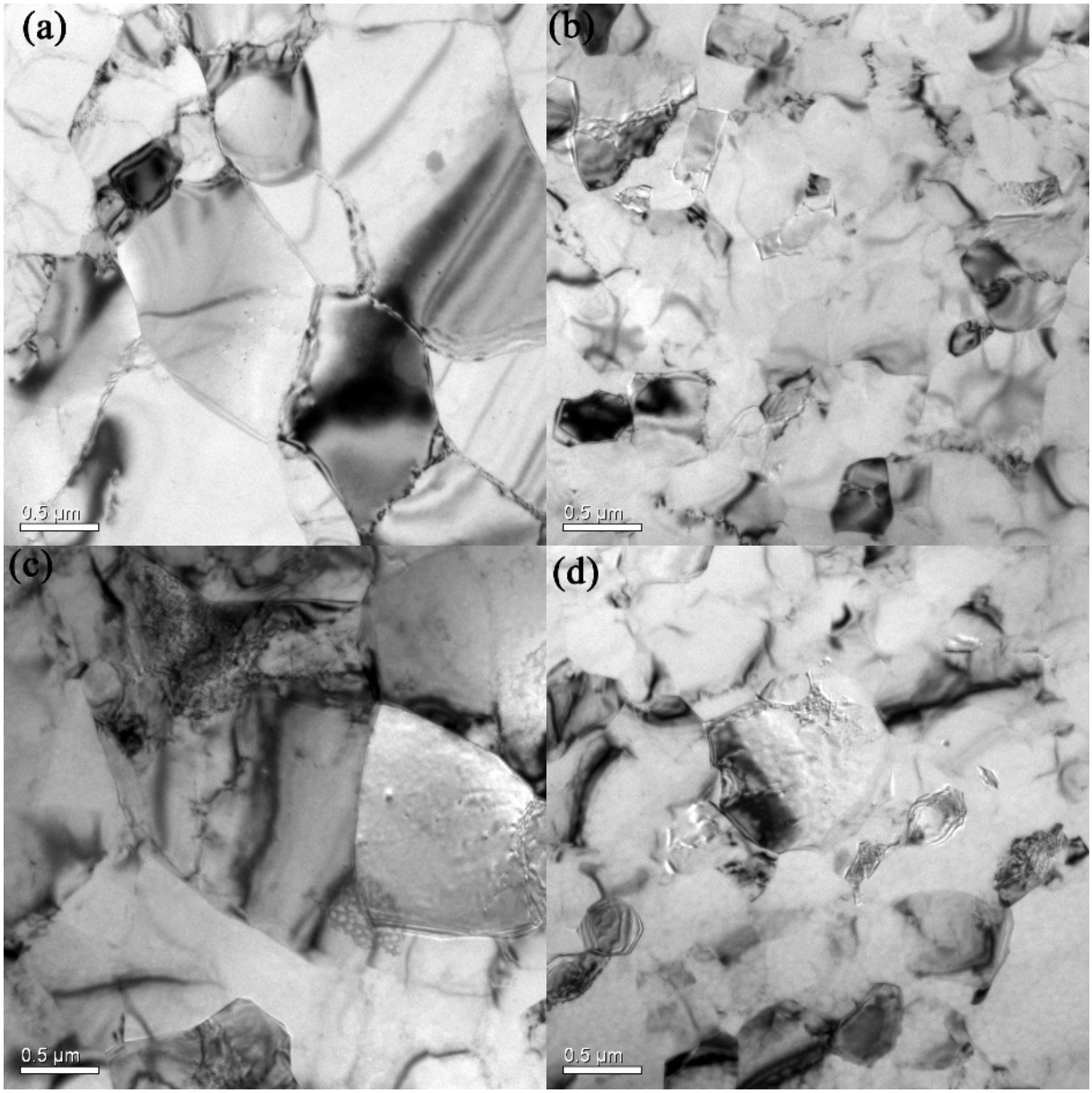

Fig. 5 TEM micrographs (bright field) of HPT processed Al–1050B: (a) at 1 mm position from centre of disk by 1T(c_0.25T) ($\varepsilon_{eq} \approx 2.4$); (b) at 4 mm position from centre of disk by 1T(c_0.25T) process ($\varepsilon_{eq} \approx 4$); (c) at 1 mm position from centre of disk by 16T(c_0.25T) ($\varepsilon_{eq} \approx 5.6$) and (d) at 4 mm position from the centre of disk by 16T(c_0.25T) process ($\varepsilon_{eq} \approx 7.1$).

4. Discussion

The present results show that cyclic HPT (c-HPT) and single reversal HPT (sr-HPT) processing influence the strengthening of commercially pure Al in a way that is significantly different from

monotonic HPT. We will first discuss the mechanisms in a qualitative manner in Section 4.1 and will describe a model that incorporates these considerations in Section 4.2.

4.1 Evolution of GNDs at the centre in the disks processed by different HPT processes

In a qualitative sense the increase in hardness with increasing deformation during m-HPT is generally ascribed to the generation of dislocations, low angle grain boundaries and/or high angle boundaries [23,28]. At and near the centre of disk the hardness increases dramatically with increasing total turns from 0.5 to 10 turns, whereas in the periphery there is only a slight increase in hardness with increasing total turns from 0.5 to 10 turns (see Fig. 2a). Fig. 2b shows that hardness increases with increasing the strain per cycle with the sample processed by m-HPT for 16 turns exhibiting the highest hardness. This trend is consistent with earlier studies on a range of metallic alloys (including Al-3%Mg-0.2%Sc alloy [13] ($x_2 = 1$), high purity Ni [14] ($x_2 \approx 0.04–0.3$), Armco iron [14] ($x_2 \cong 0.04–0.3$), Fe-0.03%C [15] ($x_2 = 0.5$) and pearlitic steel [29] ($x_2 = 0.5–4$)).

Whenever strain gradients occur, GNDs are required to accommodate the lattice curvature, and GND density increases with increasing strain gradient [18,19,20,26,30]. In the centre of the disk there is no strain, just a strain gradient. So here we expect only GNDs to occur. Near the edge of the disk a high strain in combination with a strain gradient occurs, and both GNDs and SSDs should occur. To explain the basic ideas behind the model to be outlined in the next section, we will first consider the basics of GND creation. For this we will consider a material subject to a strain gradient only, i.e. it represents the centre regions of the disk. For enhanced clarity we are here representing strain gradient in a simple form: a bending of the lattice, which would cause GNDs to extend in the direction normal to the page of the schematic drawing. In reality, in HPT, the strain gradient is different and much harder to present schematically. (GNDs would extend in the radial direction.) To explain the main findings on hardness changes in a qualitative manner we will consider four main processing situations. They are schematically illustrated in Fig. 6.

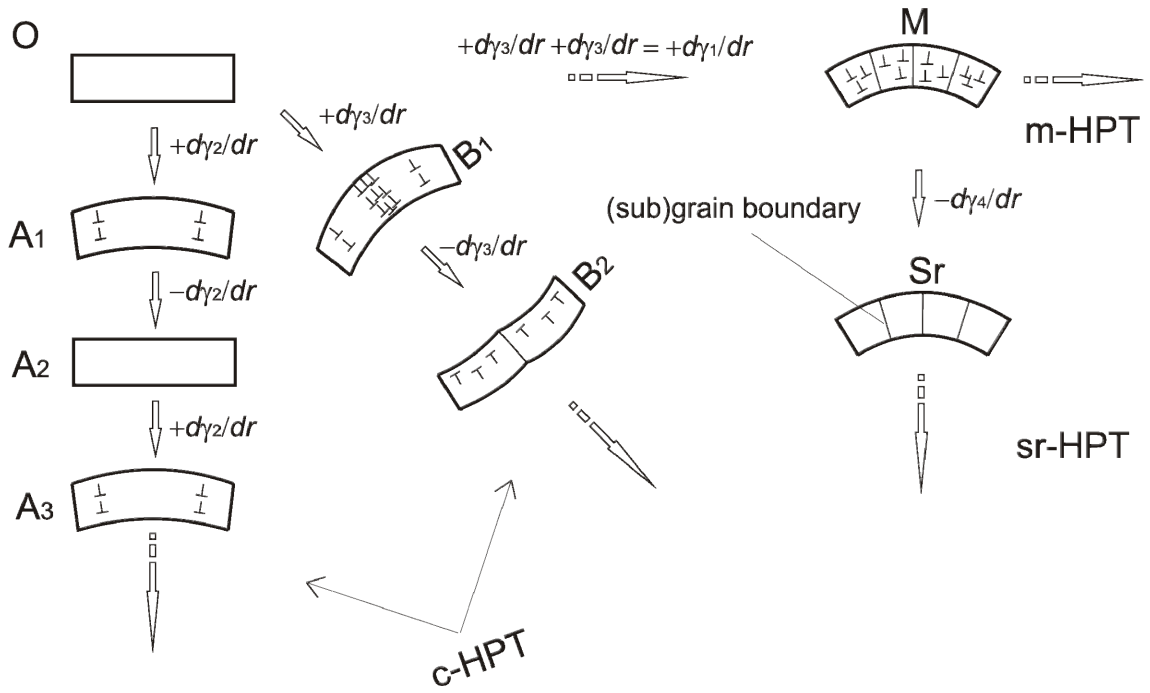

Fig. 6 Schematic illustration of the basic principles of the influence of GND creation at the centre of the m/c/sr-HPT processed disk with increasing strain.

(1) At the centre of the disk processed by m-HPT

When a grain (marked by O, initially without GNDs) is subjected to a strain gradient of + dγ_1/dr without changing the direction of deformation, the density of GNDs, ρ_{GND}, increases and when ρ_{GND} reaches a critical value, these dislocations start to come to together to form cell walls which evolve into subgrain/grain boundaries (GBs) (situation M in Fig. 6). Strengthening at the centre of the m-HTP processed disk is mainly due to the high density of GNDs.

(2) At the centre of the disk processed by c-HPT with a small reversal strain per cycle

For the grain (marked by O) subjected to a small strain gradient of + dγ_2/dr (here the strain is so small that no GBs form), the configuration of the generated GNDs is illustrated in situation A_1 (Fig. 6). We consider that, subsequently, the same strain gradient - dγ_2/dr along the opposite direction is applied on the grain. The net strain gradient is + dγ_2/dr - dγ_2/dr ('+' and '-'denotes the directions of the strain gradient). This reversal strain gradient can annihilate the GNDs from the previous strain process, and as a result ρ_{GND} decreases. The dislocation distribution is presented in Fig. 6 (situation A_2). On further changing the straining direction and deforming the

grain to the strain gradient + $d\gamma_2/dr$ - $d\gamma_2/dr$ + $d\gamma_2/dr$, the density of GNDs increases again (situation A_3). On repeating this process in several cycles only a very low density of the GNDs will result and grain refinement will be limited. (See for instance Fig. 5c.)

(3) At the centre of the disk processed by c-HPT with a large reversal strain per cycle

If the grain (marked by O) is subjected to a large strain gradient (+ $d\gamma_3/dr$), some of the generated GNDs accumulate and form GBs (situation B_1). Then, applying a reversal strain gradient of - $d\gamma_3/dr$ could destroy all the existing GNDs, but the GBs formed during the previous half cycle should be stable. The resulting ρ_{GND} and the extent of GB formation depends the magnitude of the reversal strain per cycle.

(4) At the centre of the disk processed by sr-HPT

After processing for 16 turns by m-HPT (marked by M), the disk exhibits a high density of GNDs and small grain sizes at the centre (e.g. see [24]), leading to higher hardness. During the application of the single reversal strain, the density of GNDs is initially reduced to a very low level (situation Sr) and subsequently increases again with further increasing the strain gradient.

As $d\gamma/dr$ is independent of r, GND creation is not dependent on r. But as γ increases with distance to the centre, SSDs generation will increase with r and they will dominate the development of hardness in the outer regions of the disk.

For aluminium with high stacking fault energy, at such a strain by m-HPT the cell walls could transform into well defined (sub) grain boundaries, resulting in a microstructure with fine equiaxed grains. Thus, in c-HPT, the larger the reversal strain per cycle is, the less the influence of reverse strain on strengthening due to the existing GBs. In sr-HPT, the increasing influence of SSDs with increasing r is responsible for the reduction of hardness changes induced by the reversal strain seen in Fig. 3.

4.2 A quantitative model of hardness development in HPT disks

To enhance our understanding of the strength and hardness development during HPT we propose a model that accounts for the effects of geometrically necessary dislocations and

statistically stored dislocations in strengthening of alloys processed by SPD. We will formulate the model in terms of critical resolved shear stress (CRSS) of the grains and the yield strength of the polycrystal. (Whilst we aim to achieve the best accuracy in model and related parameters, we expect that realistically an overall accuracy of the order of about 10% in hardness predictions might be the best that can be achieved in the present approach, see also Section 4.4.) To correlate yield strength to hardness we will approximate:

$$\sigma_y = 2.9Hv \tag{3}$$

where the value of 2.9 was determined as the average ratio of measured hardness and yield stress for Al-1050 at different states of (conventional) thermo-mechanical processing [31] (using data for Hv>30HV). (For this data on Al-1050 the ratio is 2.9±0.05; for other alloys this ratio may differ; for further analysis on the ratio of hardness to yield stress of metallic alloys, see [32].)

The main contributions to the yield strength are given by the expression [33,34,35]

$$\sigma_y = \sigma_0 + \Delta\sigma_{gb} + M\left(\Delta\tau_d + \Delta\tau_{sol}\right) \tag{4}$$

where σ_0 is the strength of annealed aluminium, $\Delta\tau_{sol}$ is the contribution from solution strengthening, $\Delta\tau_d$ is the strengthening due to dislocations, $\Delta\sigma_{gb}$ is the contribution due to grain boundary strengthening. M is the Taylor factor, for equiaxed grains in texture free FCC metals, Hutchinson's model gives $M = 2.6$ [36].

In the present alloys the solution strengthening is very small ($\Delta\tau_{sol}$ is estimated to be less than 5MPa), and we will here take ($M\Delta\tau_{sol}+\sigma_0$) as the yield strength of annealed 1050. The strengthening due to dislocations is given by [18,38]:

$$\Delta\tau_d = \alpha_1 Gb\sqrt{\rho} \tag{5}$$

where α_1 is constant, G is the shear modulus of aluminium (26 GPa [37]), b is the Burger's vector. The total dislocation density is the sum of the GND and SSD densities:

$$\rho = \rho_{GND} + \rho_{SSD} \tag{6}$$

At the centre of the disk the strain should be zero and hence ρ_{SSD} expected to be zero. However, the strain gradient is substantial and hence GNDs will be created. The density of GNDs is dependent only on strain gradient and length of Burger's vector, but not dependent on alloying content [18,22,32]. In an idealised geometry (considering cylindrical symmetry), the strain

gradient in HPT has only a radial component and hence the total amount of GNDs generated per unit volume is given by:

$$\rho_{\mathrm{GND,g}} = b^{-1} d\gamma / dr \,. \tag{7}$$

From Eq.2 and Eq.7, the strengthening due to these GNDs is given by [22]:

$$\Delta\tau_{\mathrm{GND}} = \alpha_1 G b \left(\frac{1}{b}\frac{d\gamma}{dr} \right)^{1/2} = \alpha_1 G \left(b \frac{d\left(2\pi N r / h\right)}{dr} \right)^{1/2} = \alpha_1 G \left(\frac{2\pi N b}{h} \right)^{1/2} \tag{8}$$

It can be seen that the strengthening due to GNDs at the centre of disk increases as $N^{1/2}$. The magnitude and distribution of strain gradient may change when changes in the microstructure occur, but this is ignored here in order to simplify the model. (And the results below will show that this simplification doesn't significantly impede accuracy of modelling predictions.)

The total amount of SSDs generated per unit volume can be expressed by [38]:

$$\rho_{\mathrm{SSD,g}} = \varepsilon \left(\frac{K_{\mathrm{A}}}{MGb\alpha_1} \right)^2 \tag{9}$$

where K_{A} is an alloy-dependent factor. The theory regarding K_{A} was recently presented [38]; for the present alloy in which solute content of the Al-rich phase is very low, K_{A} is given as:

$$K_{\mathrm{A}} = C_2 G M^{1/2} b^{1/2} \left[\frac{f}{2r_{\mathrm{p}}} \right]^{1/2} + K_{\mathrm{A}}^0 \tag{10}$$

where C_2 is a constant equalling about 0.25, f is the volume fraction of non-shearable particles and r_{p} is the average radius of the non-shearable particles and K_{A}^0 is a constant equalling about 203MPa.

As the density of dislocations in the grain increases beyond a certain critical value, dislocations will start to cluster to form cell walls, which will ultimately develop into full grain boundaries; and further dislocations can also be subsumed into existing grain boundaries. In our model we will not attempt to provide a detailed simulation of cell wall and subgrain boundary formation, which occurs at intermediate strain (about 0.3 to 1). Instead we will make the simplifying assumption that there is an effective saturation value, ρ_{sat}, for the dislocation density in a grain, (thus $\rho_{\mathrm{GND}} + \rho_{\mathrm{SSD}} \le \rho_{\mathrm{sat}}$), and that once the increasing strain has caused the dislocation density to reach this saturation value, the additional dislocations effectively being subsumed into both existing and newly forming (low angle and high angle) grain boundaries (see also [38]). Thus, on further straining beyond the stage where the critical dislocation density is reached, increasing

grain boundary strengthening dominates the further increase in hardness. (This situation will especially occur in the periphery of the HPT processed disk due to a more rapid increase of strain compared with centre region). Saturation dislocation densities were reported for several different Al alloys processed by ECAP for 8 passes [39]; the values varied with compositions from 1.8×10^{14} m^{-2} to 3.9×10^{14} m^{-2} for high purity Al and Al-1at%Mg, respectively. For our alloys, which do not contain Mg but do contain Fe and Si, we here take ρ_{sat} as 4×10^{14} m^{-2}. This is in line with an analysis of hardness and microstructure of Al-1050 processed to strain of 4 to 8 using ECAP which indicated ρ_{sat} between 3.9 to 4.1×10^{14} m^{-2} [40].

Grain boundary strengthening can be expressed by [41]:

$$\sigma_{gb} = \alpha_2 Gb\left(\frac{1}{d}\right) \tag{11}$$

d is the average grain size. The mean grain sizes, d, can be predicted using the notion that the average grain boundary misorientation angle, $\bar{\theta}$, is determined by the total number of dislocations that are subsumed in the grain boundaries per area of grain boundary [38]. As was shown in [38] a model for grain refinement can be derived if we assume that dislocation density for a mixed tilt/twist boundary can be approximated by 1.5 $S_V\theta/b$, where S_V is the area of boundaries per unit volume, θ is the misorientation angle and b is the Burgers vector. This linear relation between total amount of dislocations subsumed in grain boundaries and $\bar{\theta}$ was originally proposed by Hansen and co-workers [42,43], who applied it to low angle grain boundaries (misorientation angles typically lower than 10º). Here we will again use the approximation that this linear relation can be extended to higher dislocation angles, and we will justify this further in the Appendix. This approach then provides the relation [38]:

$$d = 4.365\frac{\bar{\theta}}{\rho_{GB}b} \tag{12}$$

where ρ_{GB} is the density of dislocation contributing to grain boundary refinement: $\rho_{GB} = \rho_{GND,g} + \rho_{SSD,g} - \rho_{sat}$.

To apply the equation the average misorientation, $\bar{\theta}$, needs to be determined. The maximum value that $\bar{\theta}$ can reach is 45° (θ_m) for a collection of randomly oriented grains [44]. We could simply take a single average value of about 22° and this will lead to reasonable predictions. (Results not presented.) For enhanced accuracy we will consider that $\bar{\theta}$ increases with

equivalent strain from an initial value of 0 to an asymptotic maximum of 45°, and that the variation can be approximated by a generic nucleation and growth equation as given in [45]:

$$\frac{\bar{\theta}}{\bar{\theta}_m} = 1 - \left((k\varepsilon)^n / \eta + 1\right)^{-\eta} \quad (13)$$

where n = 1. To determine k and η we analysed a range of data on $\bar{\theta}$ from [31,46,47,48,49, 50] (some values are based on the misorientation graphs). The results plotted in

Fig. 7 can be fitted reasonably well with the latter equation and optimised values of k = 0.3 and η = 0.5 are obtained. This function is useful and promising as it combines an asymptotic limit with initial power law behaviour, and the notion of a nucleation and impingement-limited growth which are concepts that appear to have a parallel in the present case.

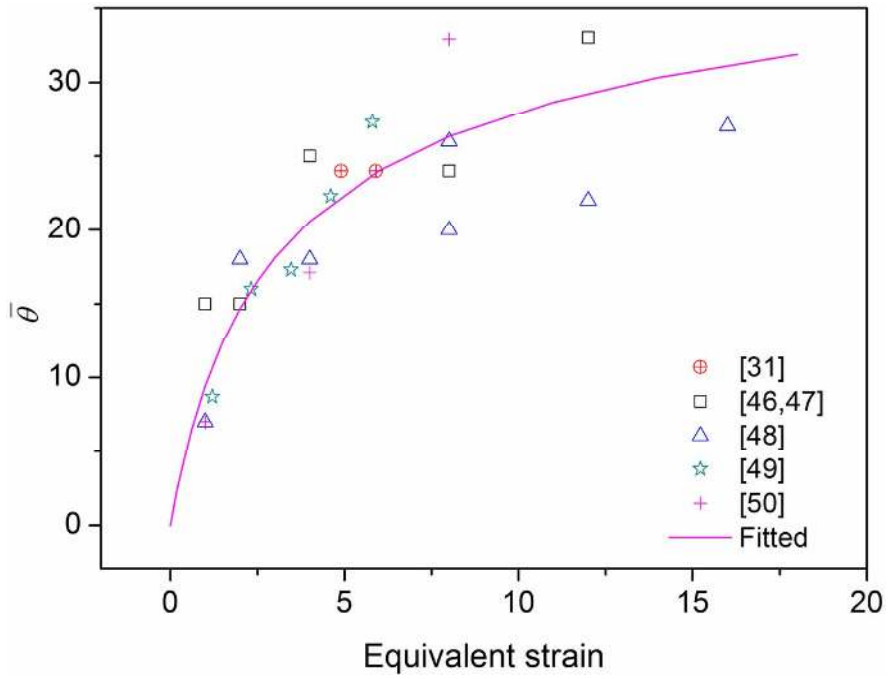

Fig. 7 Average misorientation angles obtained from several publications and a fitted curve using Eq. 13.

4.3 Hardness prediction for the centre and outer region of the disk processed by m/c-HPT

The model described above is used to make predictions of hardness, using the parameters given in Table 2. The value of K_A is determined using the model described in Eq.10, in which K_A is a function of the size of non-shearable particles and their volume density. The effective particle

diameter of 50±10 nm, is obtained from SEM analysis of etched section of HPT processed samples for 2 turns (Fig. 8). (Analysis through SEM appears to be more reliable than TEM studies of these particles, as only very few were detectable in TEM foils, and because there is some uncertainty regarding possible removal of particles during electropolishing for TEM sample preparation.)

Parameters	Value	Source
α_1	0.3	[18]
α_2	2	[41]
b	0.28 nm	[36]
ρ_{sat}	4×10^{14} m^{-2}	[39]
ρ_0	7×10^{13} m^{-2}	[51][a]
M	2.6	[36]
r_p	50 nm	From SEM (Fig. 8)
f	0.0076 (1050A), 0.0101 (1050B)	
K_A	252 MPa (1050A), 259 MPa (1050B)	Obtained from Eq. (10)
G	26 GPa	[37]
$M\Delta\tau_{sol} + \sigma_0$	28 MPa	[31]
$\bar{\theta}_m$	45°	[44]
n	1	This work
k	0.3	This work
η	0.5	This work

[a] Value is estimated from data in the reference using 15% reduction at 0.025 true strain.

Table 2 Summary of parameters used in the model

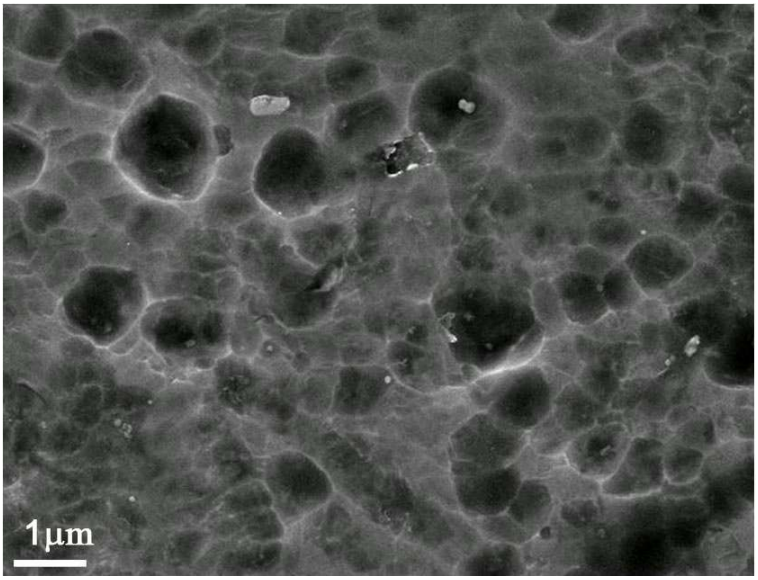

Fig. 8 FEG-SEM micrograph (SE mode) of an etched sample HPT processed to 2 turns. Note the intermetallic particles with diameter ranging from 30 to 80 nm (with an occasional larger one) and a grain size of about 0.7µm.

Right at the centre of the HPT processed disk the torsional strain is zero and no SSDs are generated. The strengthening due to dislocations is then due to GNDs only. However, it is fundamentally impossible to measure hardness at an infinitely small point as the hardness measured is effectively an average over the entire plastic zone under the indenter, and, due to small inaccuracies in placement of the indentation, it is also not realistic to expect that we can make the indentation exactly at the centre of the sample. We will account for this effect by predicting the averaged hardness over an effective area around the centre of the disk. It is estimated that effective average properties in the plastically deformed zone under the indenter are those that are encountered at the radius of the equivalent distance circle, i.e. $r = 0.4d$, where d is the diameter of the indent (i.e. d can be measured from the indent produced in as-received alloy). We will take r as the average value predicted for the sample, which works out at 15 μm. The model shows that for a region near the centre of the disk the yield strength and hardness should increase linearly with distance from the centre of the disk.

Model predictions are given in Table 3 and Fig. 9. The modelling results show an excellent correspondence between measured and predicted hardness at the centre of Al-1050A samples processed by m-HPT for different turns. (The dislocation density in extruded Al-1050 rod is taken as 7×10^{13} m^{-2} from [51].) Compared with dislocation strengthening effects, the contribution from grain boundary strengthening is relatively small (about 10 MPa by m-HPT for 10 turns). The excellent correspondence in Fig. 9 is obtained without any significant influence due to fitting of parameters, as the only fitted parameters (the 3 parameters in Eq. 13, which have a small influence on grain refinement predictions) have nearly no effect on strength predictions. Instead, it is the other parameters in Table 2, most prominently parameters that govern dislocation densities (predominantly ρ_{sat} and K_A), that have the largest influence on the strengthening predictions. All of these parameters are either known or justified in the present work and, in the case of K_A, the value was analysed and determined from measurement in [38].

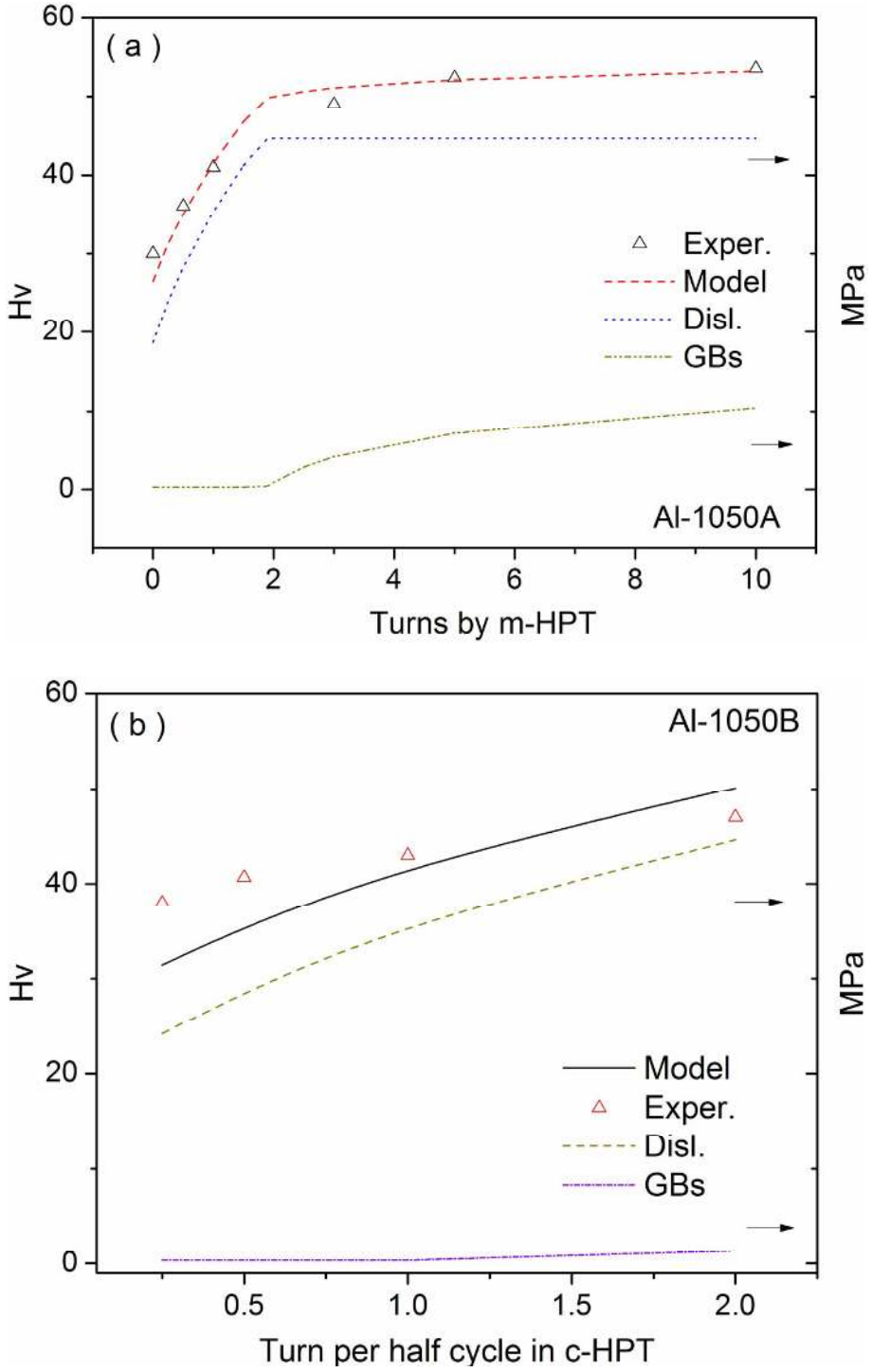

Fig. 9 Measured and predicted Hv (shown on left axis) and the strengthening due to total dislocations ($\Delta\tau_d$) and GBs (shown on right axis) for (a) the centre of m-HPT processed disks vs. turns and (b) the centre of the c-HPT processed disks vs. turns per half cycle.

Table 3 Measured hardness in the centre of disk compared with model predictions for Hv and the different strengthening components obtained from the model outlined in the section 4.3.

Alloys	Turns	$\Delta\tau_d$ (MPa)	σ_{gb} (MPa)	σ Model (MPa)	Hv Model (MPa)	Hv Exper.
Al-1050A	0	19	0.4	77	27	30
	0.5T	28	0.4	101	35	36
	1T	35	0.4	120	41	41
	3T	45	4	148	51	49
	5T	45	7	151	52	52
	10T	45	10	154.	53	54
Al-1050B	16T	45	13	157	54	63
	16T(c_0.25T)	24	0.4	91	31	38
	16T(c_0.5T)	28	0.4	102	35	41
	16T(c_1T)	36	0.4	121	42	43
	16T(c_2T)	45	1	145	50	47

With reference to Fig. 9 it is also worth noting that the model indicates that in terms of the relative increase in the individual strengthening terms (e.g. σ_{gb}(after HPT)/σ_{gb}(pre HPT), $\Delta\tau_d$(after HPT)/ $\Delta\tau_d$(pre HPT)), the grain boundary strengthening increases more strongly than the strengthening due to dislocations. However in absolute terms the strengthening due to dislocations is predicted to be the dominant strengthening mechanism in HPT processed materials. The ratio of the two strengthening contributions, e.g. $M\Delta\tau_d / \sigma_{gb}$, is high in the present model. Whilst the good model predictions obtained suggest that the model is essentially sound, further analysis is needed to confirm the $M\Delta\tau_d / \sigma_{gb}$ is correct (see also Section 4.4).

We should also note that the dislocation densities predicted in the present model, typically ranging from about 2×10^{14} m^{-2} to 4×10^{14} m^{-2}, correspond well with average dislocation densities measured in Al alloys processed by SPD to comparable strains [38,52,53,54]. This data was obtained through X-ray diffraction on relatively thick samples. Also Al alloys cold rolled to strains of about 1 show dislocation densities close to our model predictions for SPD processing to similar strain (4×10^{14} m^{-2}) [55]. TEM micrographs of thinned foils (typical TEM

foil thickness is 100 nm) of HPT processed samples generally show inhomogeneous dislocation densities, and suggest that dislocation densities in most grains is substantially lower than 10^{14} m^{-2}. We have not attempted to quantify the dislocation densities from the present TEM foils as XRD measurements of average dislocation densities available in the literature are thought to be more reliable, because TEM foil preparation is thought to substantially reduce the strain gradient in the material, and thus reduce GND densities. (An indication supporting this interpretation is found in [24] where dislocation densities in TEM samples of HPT processed Al alloys are very inhomogeneous, with some samples showing high dislocation densities over most of the electron transparent area consistent with the present model. It is also noted that in TEM investigation we tended to favour electron transparent areas that show some clearly defined features like grain boundaries and avoided areas that showed large ill-defined contrast, presumably due to extended areas with a high density of dislocations.)

Fig. 9b shows the measured and predicted Hv as a function of turn per half cycle at the centre for Al−1050B processed by c-HPT. Following the ideas outlined in Section 4.2, we assume that the effective strain is determined by the last half cycle, i.e. the effective strain is calculated by 0.25T for 16T(c_0.25T). The density of SSDs is calculated on the basis of the effective strain (Eq. 9). It is encouraging to see that even with these relatively crude assumptions (ignoring any interaction between GNDs and SSDs creation) the predictions are fairly good. The predicted contribution from dislocations increases with increasing the strain (turn) per half cycle in c-HPT. A possible explanation for the small under prediction of hardness of disk subjected to lower turns per cycle is that strain reversion of dislocations occurs during the strain reversal is not complete, and some accumulation does occur. Also the pressure applied during rotation can cause some limited increase in dislocation density.

It is also noted that the part of the model that refers to dislocation generation is the main part of a model designed to predict grain size in SPD processed alloys that was presented previously [37]. This model has been shown to accurately predict average grain size in a wide range of Al based alloys, thus providing independent support for the description of dislocation generation in the present model. Grain refinement prediction in Al-1050A (Fig. 10a), shows the grain size decreases rapidly between the centre and 0.5 mm away from the centre of HPT processed disks

and approaches a near stable value at the outer regions. (The grain size in the centre is determined by the average dislocation generation over a volume of the size of the original grain.) The model predictions in Fig. 10a indicate that the grain size at the centre of the disk will reduce from 45 micron (for as received and 1 turn samples) to 2.1 and 1.4 micron (5 and 10 turns, respectively). The grain size reduces on increasing distance from the centre. After a high number of turns the grain size is predicted to become relatively homogeneous. The predicted grain sizes in Fig. 10a are in line with those seen in TEM work [24] and our SEM work (Fig. 8) on m-HPT processed 1050. The hardness predicted for the outer regions are presented in Fig. 10b. The model predicts the dependence of hardness on number of turns well: both experimental data and model indicate an increase in hardness of about 4 Hv on increasing number of turns from 0.5 to 16.

For c-HPT, the predicted grain size and hardness in the outer regions are presented in Fig. 11. The predicted hardness is about 15% lower than the measured hardness. In view of the complex microstructure development and multiple strengthening mechanisms these levels of accuracy are considered promising. The difference might be due to an under-estimate of effective strain of c-HPT. But more likely is that the present simple assumption of a single dislocation saturation density (taken as 4×10^{14} m^{-2}) is not valid for these highly complex strain path with multiple reversals. Apparently dislocation density can increase beyond 4×10^{14} m^{-2} for c-HPT.

The single reversal strain initially decreased the hardness of m-HPT processed samples (Fig. 3). Following the above interpretations this is ascribed to the annihilation of GNDs during the single reversal strain of 0.25T. The present strengthening model predicts that the measured hardness reduction at the centre of about 12Hv is due to a halving of the total dislocation density. We are currently working on models that may explain these changes occurring on strain reversal after very high strains and strain gradients.

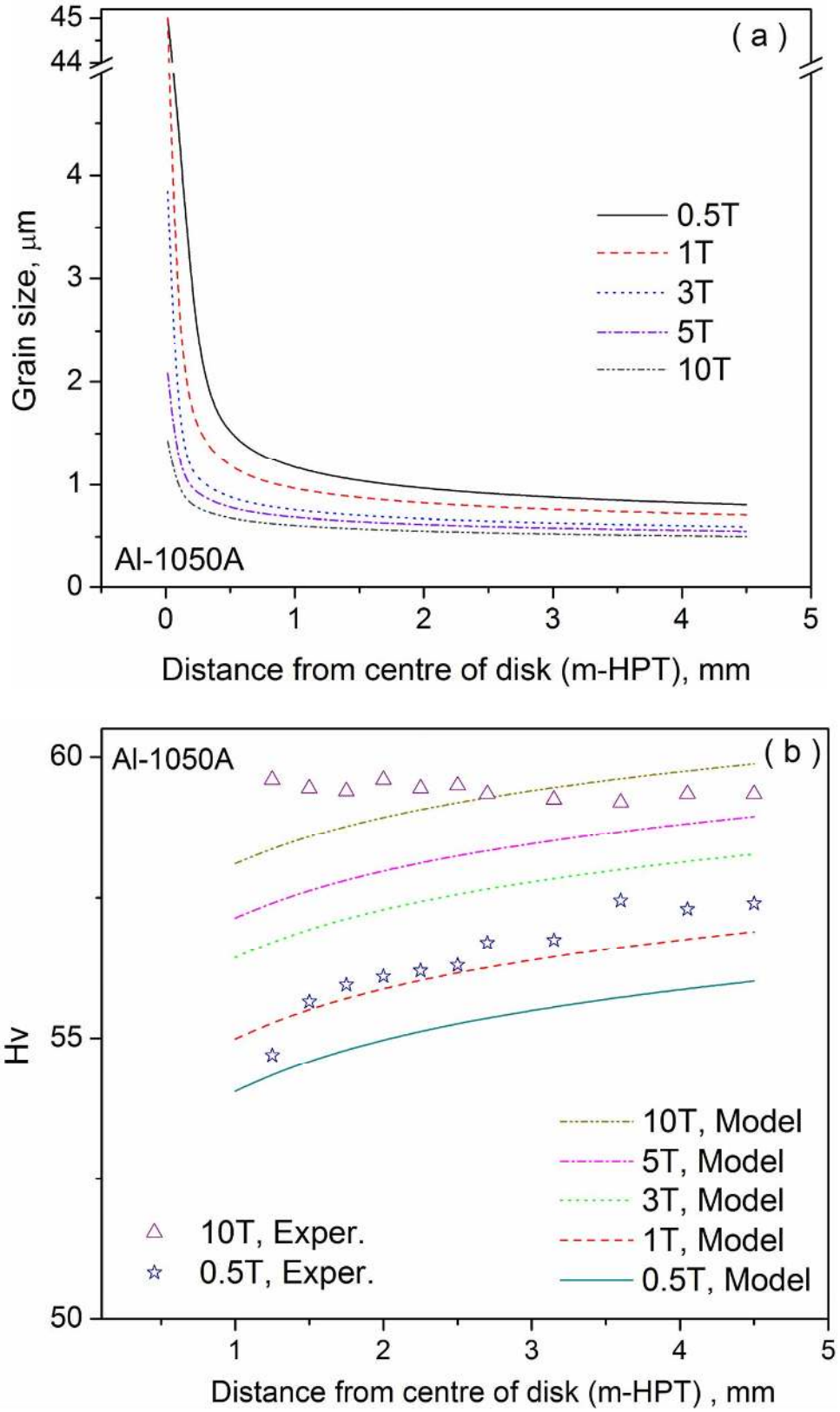

Fig. 10 (a) Predicted grain sizes vs. distance from the centre of m-HPT processed disk; (b) Measured Hv and predicted Hv of outer regions vs. distance from the centre of m-HPT processed disk.

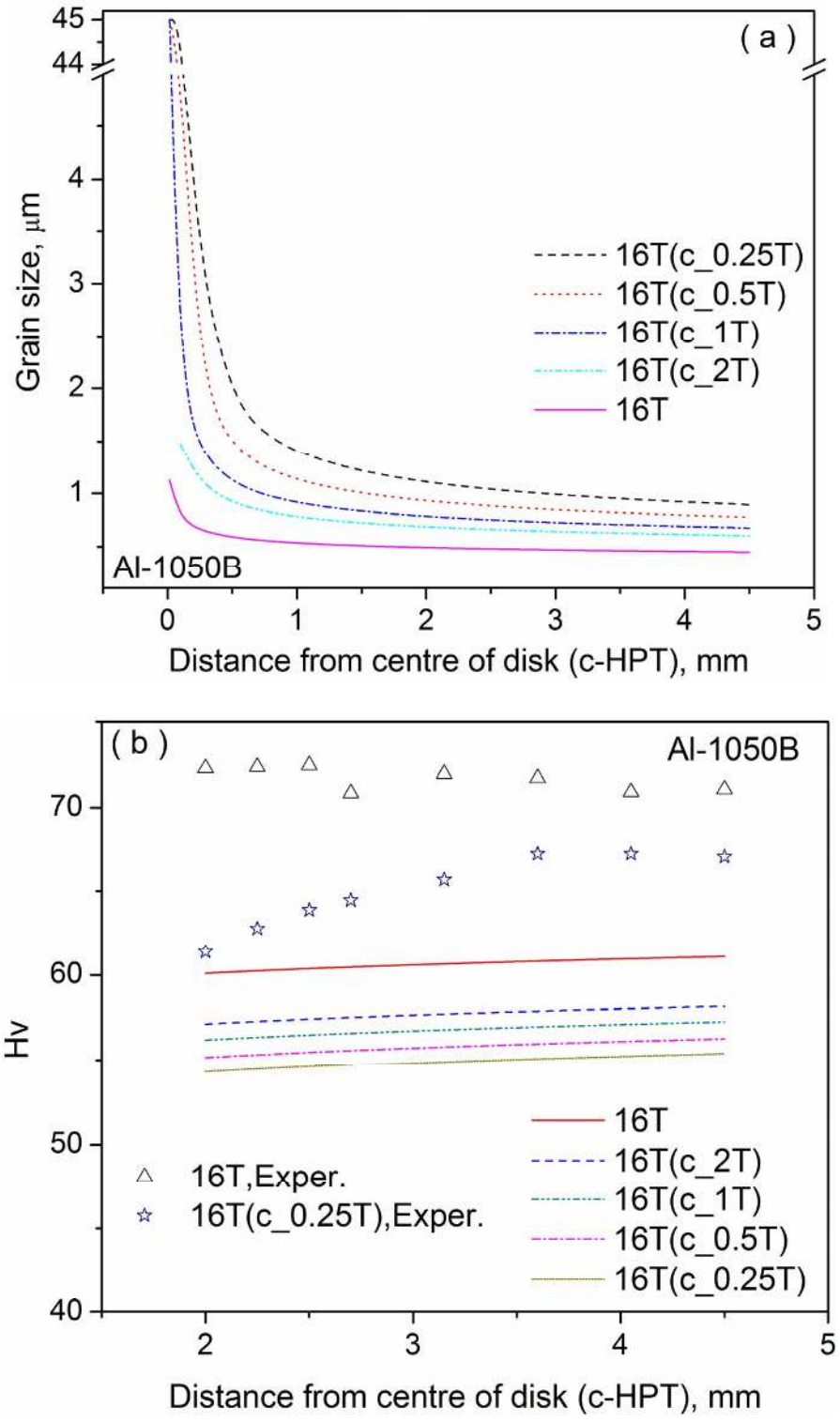

Fig. 11 (a) Predicted grain sizes vs. distance from the centre of c-HPT processed disk; (b) Measured Hv and predicted Hv of outer regions vs. distance from the centre of c-HPT processed disk.

4.4 Model accuracy and alternative modeling approaches

In the present paper we used the grain size strengthening equation (Eq 11) from [41]. This approach provides a grain size strengthening that is somewhat different from the classical Hall-Petch (see e.g. [56,57,58]) approach for the grain sizes considered here. To consider the possible influence of this on the present model we provide the following assessment. The most complete set of data for grain size dependency of flow stress for an Al-1050 alloy is provided by Hansen [58], and this data indicates a Hall-Petch constant of 25 MPa.$\mu m^{1/2}$ for strain ~0.2% and 7 MPa.$\mu m^{1/2}$ for strain 7%, with the latter strain value being a typical average strain achieved in hardness tests. Using the average on this strain range (16 MPa.$\mu m^{1/2}$) one would obtain an increase in yield strength of up to about 20 MPa and an increase in hardness of about 7 HV for the Al-1050 processed through 16 turns m-HPT, the condition for which the grain size is smallest. This hardening is comparable to the hardening calculated using Eq. 3, thus supporting the maximum hardening due grain refinement determined in Sections 4.2 and 4.3. (It is also noted that for high purity Al (>99.99%) Hall-Petch constants can be 40 to 50 MPa.$\mu m^{1/2}$ [58]. This increased Hall-Petch constant would increase the grain size strengthening effect. However, grain refinement in high purity Al during SPD is limited to about 900 nm [38], which provides an increase in yield strength of up to about 46 MPa and an increase in hardness of about 16 HV. This is still small compared to the dislocation strengthening determined in Sections 4.2 and 4.3 (see e.g. Fig. 9a).)

Related to the above we do need to note that due to potential accuracy limits in model parameters (notably r, K_A, α_2) and uncertainties related to Eqs. 3 and 11, the accuracy of the present model in terms of hardness and strength predictions is at best of the order of 10%. Nevertheless, the model captures all the main microstructural changes and hardening effects, whilst offering a semi-quantitative explanation for the softening observed on sr-HPT. To the best of our knowledge this is the first model that explains all of these observations.

Finally we should mention the alternatives to the present approach to modelling of strength of SPD processed metals. Notably, several computationally intensive methods use the evolution of

cell walls [23,25], and strain gradient effect (through the inclusion of GNDs) have been incorporated to model HPT. These models have been used to model microstructure evolution and strength during HPT in pure fcc metals [23]. As discussed before [38], our present model bypasses the cell wall evolution stage to arrive at a more computational friendly, volume averaged approach which has been shown to be suitable to predict the effect of alloying on strength evolution at high strains (typically > 3). The drawback of the present approach is that it can, as yet, not incorporate these cell walls which are important at the intermediate stage. Instead, in our approximation, this stage is modelled using grain boundaries that are infinitely thin having a low misorientation.

5. Conclusions

In the present study, the influence of strain reversal on strengthening in high pressure torsion (HPT) process was investigated using commercially pure aluminium. The Vickers microhardness was evaluated on different HPT processed samples. The experiments included m-HPT, c-HPT and single reversal HPT (sr-HPT) in which a severe unidirectional HPT deformation (here 16 turns) is followed by a single reversal for a small number of turns. The following main conclusions can be drawn:

The microhardness at the centre of commercially pure aluminium disk processed by m-HPT increased dramatically with increasing the strains. In contrast, only very limited increase in microhardness at the centre of the disk subjected to cyclic HPT (c-HPT) was observed. The strengthening effect can be improved with increasing the strain per cycle in c-HPT. At the centre of the disk grain refinement is limited.

These results were explained by a model based on GNDs and SSDs, incorporating grain refinement. A key element of the model is the assumption that at the very high strains developed in severe plastic deformation processes such as HPT the dislocation density reaches a saturation value.

The model quantitatively explains the main observations for the hardness changes in the different HPT processes. The model shows that the strength / hardness is predominantly due to GNDs and SSDs, with grain refinement providing less than 10% of the strengthening effect. The model fits the measured hardness at and near the centre and in the periphery of the disk well.

The results from sr-HPT experiments show a remarkable drop in hardness at the centre. Whilst no quantitative model is available for this, the present analysis indicates that GNDs dominate the strengthening at the centre of the disk and that on strain reversal substantial elimination occurs.

Acknowledgements

This work was partially supported by EPRSC under Grant No EP/D00313X/1. One of the authors (JWZ) thanks the China Scholarship Council (CSC) for financial support. Dr S.C. Wang is gratefully acknowledged for assistance with TEM, Dr X.G. Qiao for valuable discussions on grain boundary misorientations and dislocation densities, Mr Nimi Finecountry for assistance with sample etching and SEM.

Appendix

The relation between dislocation density in a cell wall or low angle grain boundary and the misorientation between the grains as given by Hansen and co-workers [41,42], and adopted in the present work, was originally provided in the context of boundaries / cell walls with low misorientation angles [41,42]. As misorientation angles increase to the typical values observed after SPD of about 30º we can expect that deviations will be introduced. To estimate the magnitude of the deviations we can compare the expressions for misorientation angles for the case of dislocation that are parallel to grain boundaries. In this case the low angle approximation is [59]:

$$b/s \cong \theta \qquad \text{(A1)}$$

where s is the average distance between dislocations. The linear relation between θ and $1/s$ is analogous to the Hansen approach. For higher angle misorientation several relations have been suggested [60,61]:

$$b/s = 2\sin(\theta/2) \quad \text{(A2)}$$

or [62]

$$b/s = 2\tan(\theta/2) \quad \text{(A3)}$$

or [57]

$$b/s = 2\sin(\theta) \quad \text{(A4)}$$

or [63]

$$b/s = \tan\theta \quad \text{(A5)}$$

The differences in the expressions are due primarily to different assumptions on the arrangement of dislocations in the grain boundary. To the best of our knowledge a conclusive analysis as to which of these expressions (A2-A5) is more accurate is not available.

If we calculate the deviations introduced by the various approximations for a typical θ of about 30º we find deviations of 1%, -2%, 4% and 10% between Eq 1 on the one hand and Eqs A2, A3, A4, and A5, respectively. Thus we can expect that the adoption of the linear relation between total amount of dislocations subsumed in the grain boundary and θ, our model has an uncertainty in prediction of grain size of about 2 to 4%, increasing to 10% if A5 is the correct approximation. (Such deviations are within the 22% accuracy in grain size predictions shown in [37].) Following Eq. 11 the uncertainties in prediction of strengthening due to grain boundaries amount to the same percentages, which typically amounts to 0.2 to 0.4 HV (increasing to 1HV if A5 is the correct approximation) for grains sizes typical of the highest strains reported in the

present paper. Clearly, such deviations are very limited, and do not significantly influence analysis and conclusions presented in Sections 4 and 5. For further refinement of model predictions, first a conclusive analysis of the validity of A2-A5 needs to be performed.

References

[1] R.Z. Valiev, Y. Estrin, Z. Horita, T.G. Langdon, M.J. Zehetbauer, Y.T. Zhu, JOM 58 (2006) 33–39.
[2] V.M. Segal, Mater. Sci. Eng. A 197 (1995) 157-164.
[3] M. Furukawa, Y. Iwahashi, Z. Horita, M. Nemoto, T.G. Langdon, Mater. Sci. Eng. A 257 (1998) 328–332.
[4] N. Tsuji, Y. Saito, H. Utsunomiya, S. Tanigawa, Scripta Mater. 40 (1999) 795–800.
[5] M. Richert, H.P. Stuwe, J. Richert, R. Pippan, C. Motz, Mater. Sci. Eng. A 301 (2001) 237–243.
[6] A. Belyakov, T. Sakai, H. Miura, K. Tsuzaki, Phil. Mag. A 81 (2001) 2629– 2643.
[7] P.W. Bridgman. Studies in large plastic flow and fracture, 1952,McGraw-Hill, New York, NY, USA.
[8] A.P. Zhilyaev, T.G. Langdon, Prog. Mater. Sci. 53 (2008) 893–979.
[9] L.S. Toth, M. Arzaghi, J.J. Fundenberger, B. Beausir, O. Bouaziz, R. Arruffat-Massion, Scripta Mater 60 (2009) 175–177.
[10] R. Lapovok, A. Pougis, V. Lemiale, D. Orlov, L.S. Toth, Y. Estrin, J. Mater. Sci. 45 (2010) 4554–4560.
[11] R. Kocich, M. Greger, M. Kursa, I. Szurman, A. Macháčková, Mater. Sci. Eng. A, 521 (2010) 6386–6392.
[12] C. Xu, Z. Horita, T.G. Langdon, J. Mater. Sci. 43 (2008) 7286–7292.
[13] Z. Horita,T.G. Langdon, Mater. Sci. Eng. A 410–411 (2005) 422–425.
[14] F. Wetscher, R. Pippan, Phil. Mag. 6 (2006) 5867–5883.
[15] Y. Todaka, M. Umemoto, A. Yamazaki, J. Sasaki, K. Tsuchiya, Mater. Trans. 49 (2008) 47–53.
[16] M. Kawasaki, T.G. Langdon, Mater. Sci. Eng. A 498 (2008) 341–348.
[17] D. Orlov, Y. Todaka, M. Umemoto, N. Tsuji, Mater. Sci. Eng. A 499 (2009) 427–433.
[18] M.F. Ashby, Phil. Mag. 21 (1970) 399–424.
[19] E. Aifantis, J. Eng. Mater. Techn. 106 (1984) 326.
[20] N.A. Fleck, J.W. Hutchinson, J. Mech. Phys. Solids 41 (1993) 1825.
[21] D. Setman, E. Schafler, E. Korznikova,M.J. Zehetbauer, Mater. Sci. Eng. A 493 (2008) 116-122.
[22] Y. Todaka, M. Umemoto, Y.Z. Liu, K. Tsuchiya, Mater. Sci. Eng. A 462 (2007) 264–268.
[23] Y. Estrin, A. Molotnikov, C.H.J. Davies, R. Lapovok, J. Mech. Phys. Solids 56 (2008) 1186–1202.
[24] J.W. Zhang, N. Gao, M.J. Starink, Mater. Sci. Eng. A 527 (2010) 3472-3479.
[25] E. Hosseini, M. Kazeminezhad, J. Mater. Sci. 44 (2009) 1212-1218.
[26] L.S. Toth, Y. Estrin, R. Lapovok, C. Gu, Acta Mater. 58 (2010) 1782-1794.
[27] N.H. Polakowski, E.J. Ripling, Strength and structure of engineering materials. Englewood Cliffs, NJ: Prentice-Hall, 1966.
[28] A. Vorhauer, R. Pippan, Scripta Mater. 51 (2004) 921–925.
[29] F. Wetscher, B. Tian, R. Stock, R. Pippan, Mater. Sci. Forum 503 (2006) 455–460.
[30] N.A. Fleck, G.M. Muller, M.F. Ashby, J.W. Hutchinson, Acta Metall Mater 42 (1994) 475-487.

[31] X.G Qiao, M.J. Starink, N. Gao, Mater. Sci .Eng. A 513 (2009) 52–58.
[32] X.G. Qiao, N. Gao, M.J. Starink, Acta Mater. 58 (2010) 3690–3700.
[33] M.J. Starink, S.C. Wang, Acta Mater. 51 (2003) 5131.
[34] M.J. Starink, A. Deschamps, S.C. Wang, Scripta Mater. 58 (2008) 377–382.
[35] M.J. Starink, S.C. Wang, Acta Mater. 57 (2009) 2376–2389.
[36] J.W. Hutchinson, Proc. R. Soc. London A 319 (1970) 247–272.
[37] J.R. Kissel, R.L. Ferry, Aluminium Structures: A guide to their specifications, Design, second ed. New York: John Wiley & Sons, 2002.
[38] M.J. Starink,X.G. Qiao, J.W. Zhang, N. Gao, Acta Mater. 57 (2009) 5796–5811.
[39] J. Gubicza, N.Q. Chinh, T. Csanadi, T.G. Langdon, T. Ungar, Mater. Sci. Eng. A 462 (2007) 86–90.
[40] X.G. Qiao, PhD Thesis, University of Southampton, UK, 2010.
[41] E. Nes, T. Pettersen, K. Marthinsen, Scripta Mater. 43 (2000) 55–62.
[42] N. Hansen, Scripta Mater. 51(2004) 801.
[43] J.R. Bowen, P.B. Prangnell, D.J. Jensen, N. Hansen, Mater. Sci. Eng. A 387–389 (2004) 235
[44] J.K. Mackenzie, M.J. Thomson MJ, Biometrika 44 (1957) 205–210.
[45] M.J. Starink, Int. Mater. Rev. 49 (2004) 191–226.
[46] E.A. El-Danaf, Mater. Sci. Eng. A 487 (2008) 189–200.
[47] E.A. El-Danaf, M.S. Soliman, A.A. Almajid, M.M. El-Rayes, Mater. Sci. Eng. A 458 (2007) 226–234.
[48] Q. Liu, X. Huang, D.J. Lloyd, N. Hansen, Acta Metall. 50 (2002) 3789–3802.
[49] M. Reihanian,R. Ebrahimi, M. Moshksar, D. Terada, N. Tsuji, Mater. Character. 59 (2007) 1312–1323.
[50] A.P. Zhilyaev, T.R. McNelley, T.G. Langdon, J. Mater. Sci. 42 (2007) 1517–1528.
[51] C. Merriman, D.P. Field, P. Trivedi, Mater. Sci. Eng. A 494 (2008) 28–35.
[52] Reihanian M, Ebrahimi R, Moshksar MM, Terada D, Tsuji N. Mater Char 59 (2008)1312.
[53] Gubicza J, Chinh NQ, Krallics Gy, Schiller I, Ungar T. Current Applied Physics 6 (2006) 194.
[54] Chowdhury SG, Mondal A, Gubicza J, Krallics G, Fodor A. Mater Sci Eng A 409 (2008) 335.
[55] S.C. Wang, Z. Zhu, M.J. Starink, J. Microscopy 217 (2005) 174–178.
[56] E.O. Hall, Proc Phys Soc Sect B 64 (1951), 747.
[57] N.J. Petch, J Iron Steel Inst 26 (1953), 601..
[58] N. Hansen, Acta Metall. 25 (1977) 863-869.
[59] A.W. Sleeswyk, Acta Metall. 11 (1963) 1192-1193
[60] W.T. Read, Dislocations in Crystals, McGraw-Hill, New York (1953) p.158.
[61] J. Friedel, Les Dislocations, Gauthier-Villars, Paris (1956) p.180.
[62] A.H. Cottrell, Dislocations and Plastic Flow in Crystals, Clarendon, Oxford (1953) p.90.
[63] Y. Estrin, L.S. Tóth, Y. Brechet, H.S. Kim, Mater. Sci. Forum 503–504 (2006) 675.